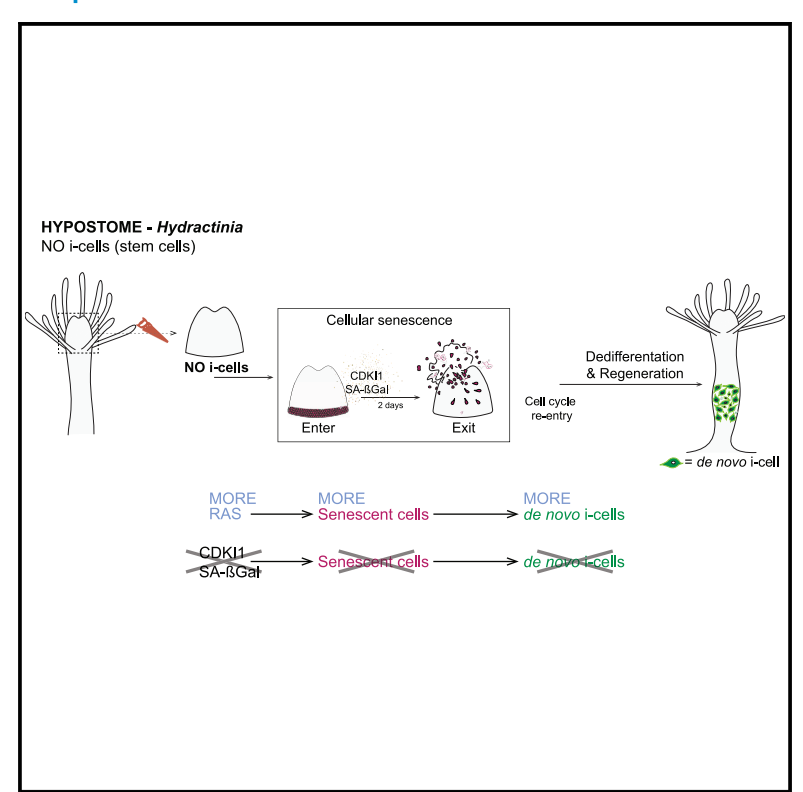
# Senescence-induced cellular reprogramming drives cnidarian whole-body regeneration

#### **Graphical abstract**



#### **Authors**

Miguel Salinas-Saavedra, Febrimarsa, Gabriel Krasovec, Helen R. Horkan, Andreas D. Baxevanis, Uri Frank

#### Correspondence

uri.frank@universityofgalway.ie

#### In brief

Cellular senescence is a form of permanent cell-cycle arrest in animals that is associated with aging and inflammation. Salinas-Saavedra et al. find that, in the absence of resident stem cells, senescent cells can instruct neighboring somatic cells to reprogram into stem cells that drive whole-body regeneration in the cnidarian *Hydractinia* symbiolongicarpus.

#### **Highlights**

- Amputation injury induces senescence in a small number of head cells in Hydractinia
- Senescent cells persist in the tissue for several hours before being expelled
- Signals emitted by senescent cells induce reprogramming of neighboring cells
- Reprogrammed cells proliferate and drive whole-body regeneration







#### **Article**

# Senescence-induced cellular reprogramming drives cnidarian whole-body regeneration

Miguel Salinas-Saavedra, <sup>1</sup> Febrimarsa, <sup>1</sup> Gabriel Krasovec, <sup>1</sup> Helen R. Horkan, <sup>1</sup> Andreas D. Baxevanis, <sup>2</sup> and Uri Frank <sup>1</sup>, <sup>3</sup>, \*

<sup>1</sup>Centre for Chromosome Biology, School of Biological and Chemical Sciences, University of Galway, Galway, Ireland

<sup>2</sup>Computational and Statistical Genomics Branch, Division of Intramural Research, National Human Genome Research Institute, National Institutes of Health, Bethesda, MD 20892, USA

3I ead contact

\*Correspondence: uri.frank@universityofgalway.ie https://doi.org/10.1016/j.celrep.2023.112687

#### **SUMMARY**

Cell fate stability is essential to maintaining "law and order" in complex animals. However, high stability comes at the cost of reduced plasticity and, by extension, poor regenerative ability. This evolutionary trade-off has resulted in most modern animals being rather simple and regenerative or complex and non-regenerative. The mechanisms mediating cellular plasticity and allowing for regeneration remain unknown. We show that signals emitted by senescent cells can destabilize the differentiated state of neighboring somatic cells, reprogramming them into stem cells that are capable of driving whole-body regeneration in the cnidarian *Hydractinia symbiolongicarpus*. Pharmacological or genetic inhibition of senescence prevents reprogramming and regeneration. Conversely, induction of transient ectopic senescence in a regenerative context results in supernumerary stem cells and faster regeneration. We propose that senescence signaling is an ancient mechanism mediating cellular plasticity. Understanding the senescence environment that promotes cellular reprogramming could provide an avenue to enhance regeneration.

#### **INTRODUCTION**

Regenerative abilities in animals are irregularly scattered among taxa but are largely inversely correlated with their structural complexity. With some exceptions, morphologically simple animals such as sponges, cnidarians, and planarians can regenerate whole bodies from tissue fragments, while complex animals such as vertebrates have more limited capabilities to restore lost body parts. Regeneration requires a certain level of growth plasticity that can be realized by a resident pool of stem cells or by mechanisms that induce reprogramming of differentiated cells to provide proliferative progenitors. However, the high plasticity that allows for whole-body regeneration may also compromise the integrity of complex structures and increase malignancy risk. Therefore, high plasticity and structural/morphological complexity rarely co-occur in one species.

A major question arising from this line of arguments concerns the nature of the mechanisms that mediate cellular plasticity in regenerative animals. If regeneration was a primitive trait in metazoans, these mechanisms have been lost or became ineffective in non-regenerative taxa. Therefore, studying animals with high regenerative abilities could provide insight into the lack of regeneration in other animals. In the long term, this information might be harnessed to induce plasticity in complex, non-regenerative animals, enhancing their regenerative abilities under controlled conditions.

Studying regeneration in a cnidarian, we show that senescence signaling can drive somatic cell reprogramming in a

regenerative context. Our results, combined with data from regeneration studies in other animals, suggest that senescence is an ancient mechanism in metazoans used to convey a stress signal to surrounding tissues, thereby driving a regenerative response. We propose that the ability to respond to a senescence signal is one of the factors underlying differential regenerative abilities in modern metazoans.

#### **RESULTS**

### Stem-cell-less tissues can regenerate whole animals that include stem cells

The cnidarian *Hydractinia* symbiolongicarpus—a relative of jellyfishes and corals—is a highly regenerative animal that is able to regrow a lost head within 3 days post amputation (dpa).<sup>5,6</sup> Hydractinia head regeneration is driven by a population of adult, pluripotent migratory stem cells, known as i-cells, that are normally restricted to the lower body column of the animal and can differentiate into both somatic cells and gametes. These i-cells, which can easily be visualized via Piwi1 expression, migrate to the injury site post amputation to restore the head. However, the heads of uninjured animals are devoid of i-cells (Figure 1A),5 so the head alone would not be expected to be able to regenerate a new body due to its lack of i-cells. Surprisingly, we have discovered that the amputated oral tips of heads (known as hypostomes) can indeed regenerate into a fully functional animal (Figure 1B) that contains i-cells, despite having no i-cells immediately post amputation (Figures 1C and S1A). We termed







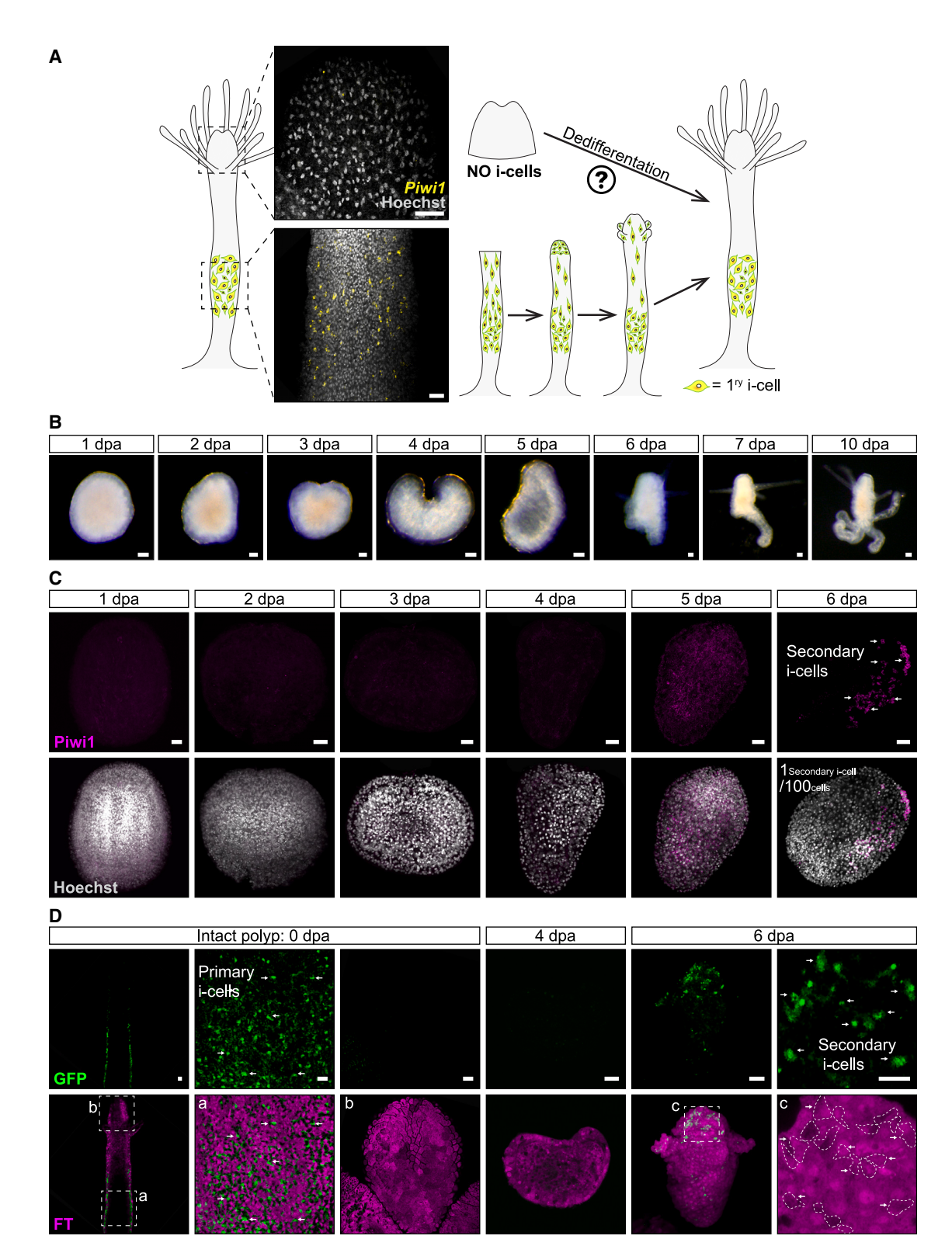


Figure 1. Secondary i-cells emerge in amputated hypostomes 6 dpa

(A) Piwi1 mRNA signal amplification by exchange reaction (SABER)-fluorescence in situ hybridization (FISH) of an intact Hydractinia polyp. Primary i-cells are restricted to the lower part of the body but are absent from the hypostome.

(B) Amputated hypostomes can regenerate a fully functional animal within 6–10 dpa.

#### **Article**



the i-cells that appeared de novo in regenerating hypostomes "secondary i-cells," as opposed to primary i-cells that are generated during embryogenesis.

To visualize the process of secondary i-cell appearance in vivo, we generated a Piwi1 transgenic reporter animal that expressed a Fast-FT mCherry timer protein<sup>9</sup> and membrane GFP under the control of the Piwi1 genomic control elements. 5 Fast-FT exhibits time-dependent blue-to-red chromophore maturation. The immature Fast-FT mCherry protein could not be observed under our microscopes due to the lack of a commercial filter, but i-cells expressing a bright green membrane GFP could be viewed in the live translucent animal. Mature red Fast-FT mCherry protein was readily visible in differentiated cells (Figures 1D, and S2). The reporter transgene is silenced during differentiation, resulting in the early progeny of i-cells becoming red due to maturation of the Fast-FT mCherry protein and dim green due to the GFP's halflife (Figures 1D and S2B-S2C). Hypostomes were then isolated from transgenic Piwi1 reporter animals and examined under a fluorescence microscope to exclude the presence of any bright green i-cells; these hypostomes were then incubated in seawater (Figure 1D). Consistent with the experiments described above, GFP+ i-cells reappeared, de novo, at 6 dpa in an otherwise mature red mCherry<sup>+</sup> background (Figures 1D and S2D). Hence, we concluded that, following amputation, a yet unknown mechanism induces the reprogramming of differentiated somatic cells back to Piwi1+ i-cells that then drive whole-body

Intact Hydractinia hypostomes lack i-cells and cycling cells.5 Based on EdU incorporation, we established that a wave of DNA synthesis occurs between 3 and 4 dpa (Figures 2A and \$1B). Secondary Piwi1<sup>+</sup> i-cells appeared in the hypostome tissue around 6 dpa (Figure 1). These cells had residual EdU signals, showing that they were derived from cells that were in S-phase 2 days earlier (Figures 2B and S1B). Treating hypostomes with hydroxyurea to arrest cells in S-phase did not completely abolish the upregulation of Piwi1 in some cells (Figure 2C). However, the level of Piwi1 expression in these cells was low compared with i-cells assessed using immunofluorescence. Moreover, hydroxyurea-treated hypostomes did not regenerate and subsequently died, showing that proliferation occurring before secondary i-cell appearance is essential for complete reprogramming of somatic cells to fully functional i-cells.

To verify that somatic cells undergo reprogramming to give rise to secondary i-cells, we amputated hypostomes from a  $\beta$ -tubulin::Fast-FT transgenic reporter animal. These animals express mCherry in all differentiated cells but not in i-cells.8 We allowed the hypostomes to develop secondary i-cells and then fixed and stained them with antibodies raised against Piwi1 and mCherry. We found cells that were double-positive, showing that cells that had expressed mCherry in the transgenic reporter animal (i.e., differentiated cells) reprogrammed into Piwi1+ i-cells (Figures 2D and S3A).

The Hydractinia main body axis is generated and maintained by Wnt/β-catenin signaling. 10,11 We used a Wnt3 transgenic reporter animal that expresses GFP in the oral-most tip of the hypostome<sup>8</sup> to dynamically follow the polarity of the isolated hypostomes. We found that GFP expression in the reporter animal lost its oral focus within 2-3 dpa, spreading around the tissue (Figures 2E, S3B, and S3C). We repeated the experiment with an Rfamide transgenic reporter animal that expresses GFP in a stereotypic fashion in the nervous system of the head. As with the Wnt3 reporter, within 2-3 dpa, the GFP+ neurons lost their typical oral orientation and became disorganized (Figures 2F, S3D, and S3E). We concluded that axis polarity is lost in isolated hypostomes within 3-4 dpa. Following secondary i-cell appearance, the hypostomes elongated and regained polarity, as visualized by Wnt3 and Rfamide expression in transgenic reporter animals (Figures 2E-2F, S3C, and S3E; 6 dpa), developing into intact yet small animals.

#### Senescence precedes regenerative reprogramming

We then aimed to identify the nature of the signal that induces the appearance of secondary i-cells in isolated hypostomes that were initially devoid of i-cells. We hypothesized that this signal is present in regenerating tissues a few days before both reprogramming and the emergence of secondary i-cells. Therefore, we extracted RNA from amputated hypostomes 0, 1, 3, and 6 dpa and sequenced their transcriptomes. Using CellAgeDB12 as a reference, we collected sequences of 279 cell senescenceassociated proteins from UniProt. We identified Hydractinia homologs for 229 of these proteins using reciprocal BLAST. Of these 229 homologs, we found that 142 genes were significantly differentially expressed in at least one time point when compared with the preceding time point. We plotted the results of the candidate gene search as a heatmap (Figure 2G), identifying a burst of differential expression in cell senescence-associated genes on 1 dpa, which is reduced 3 dpa and further reduced 6 dpa (Data S1).

Senescence is a form of irreversible cell-cycle arrest in animals, induced by stress, damage, oncogene expression, or telomere attrition. 13,14 Senescent cells secrete a cocktail of factors, collectively known as the senescence-associated secretory phenotype (SASP)<sup>15</sup>; these factors induce inflammation and enhance senescence and malignancy in neighboring cells. 15,16 Long-term accumulation of senescent cells in tissues is thought to contribute to organismal aging.<sup>17</sup> Conversely, a role for senescence (and short-term senescence in particular) in cellular plasticity has been reported in mammals and other vertebrates. 16,18-20 However, its natural context of action is not well understood. We hypothesized that amputation injury induces senescence in some cells that then emit a signal (through

<sup>(</sup>C) Piwi1 antibodies detect secondary i-cells in hypostomes, 6 dpa (arrows). On average, we observed 1 secondary i-cell per 100 cells.

<sup>(</sup>D) In vivo imaging of primary and secondary i-cells (arrows) in a Piwi1: Fast-FT reporter animal. In the intact polyp, primary i-cells (GFP+) do not overlap with the FT red fluorescence and are absent from the hypostome. However, in amputated hypostomes, secondary i-cells emerging at 6 dpa (depicted with arrows and dashed lines) overlap with the FT red fluorescence (C) observed at 4 dpa. Tissues do not express GFP at 4 dpa. This shows the reprogramming of somatic cells to secondary i-cells. Scale bars: 20 μm.



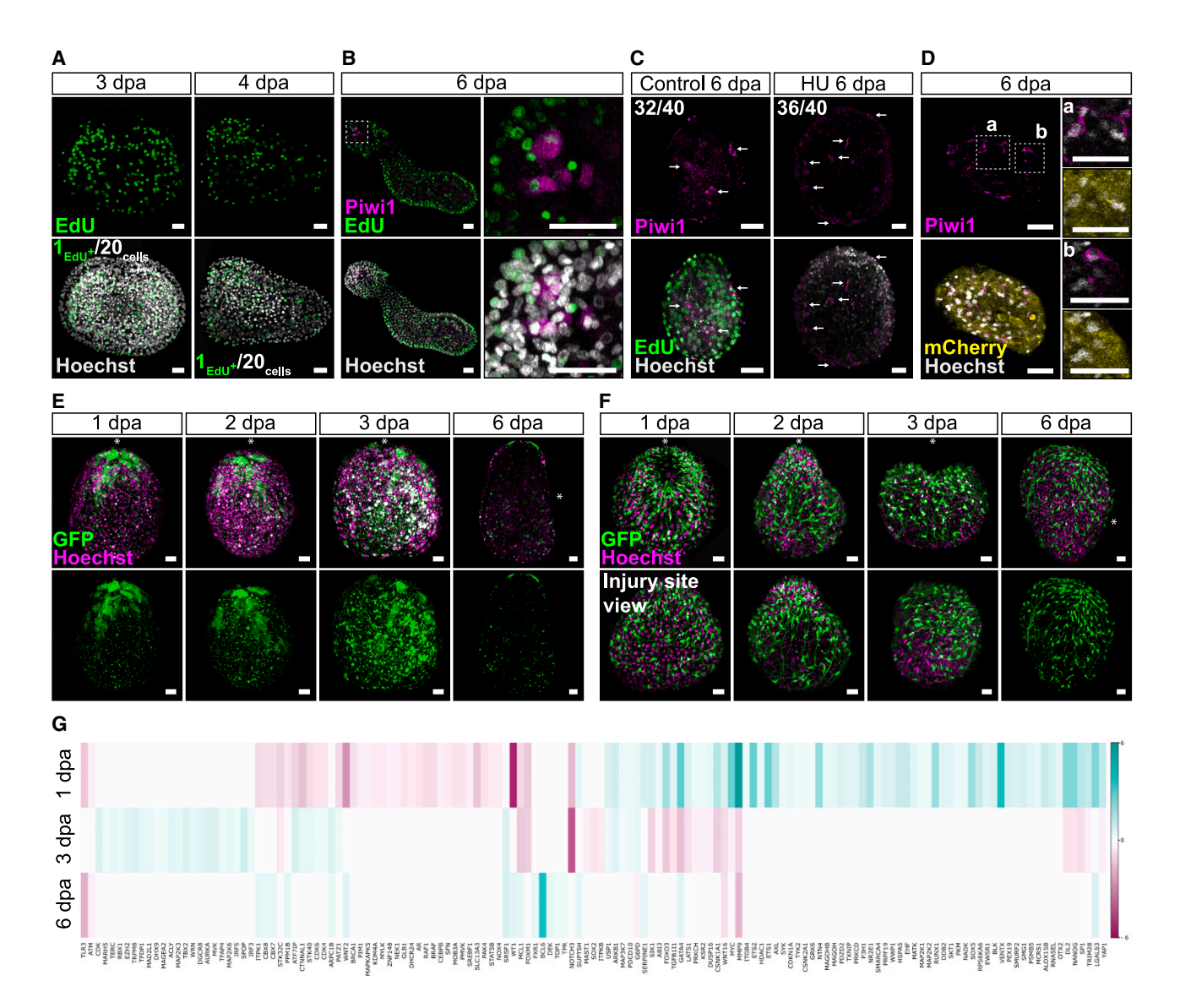


Figure 2. Cellular and molecular events accompanying whole-body regeneration from amputated hypostomes

- (A) Cell-cycle re-entry (EdU incorporation) takes place between 3 and 4 dpa. On average, we observed 1 EdU+ cell per 20 cells.
- (B) Piwi1<sup>+</sup> cells have residual EdU signals at 6 dpa after being incubated in EdU for 48 h between 3 and 4 dpa.
- (C) Only few Piwi1<sup>+</sup> cells appear in hydroxyurea-treated hypostomes but do not cycle.
- (D) Piwi1<sup>+</sup> cells are also mCherry<sup>+</sup>, indicating the reprogramming of adult somatic cells.
- (E) In vivo imaging of amputated hypostomes from a Wnt3:GFP reporter animal 1, 2, 3, and 6 dpa. Bottom panels show the GFP channel only. Asterisks indicate the oral pole pre-amputation.
- (F) In vivo imaging of amputated hypostomes from an RFamide:GFP reporter animal. Bottom panels show the site of amputation. Asterisks indicate the oral pole
- (G) Heatmap showing senescence-associated genes are highly differentially expressed at 1 dpa and less so at 3 and 6 dpa. Scale bars: 20 µm. See also Figures S1 and S3.

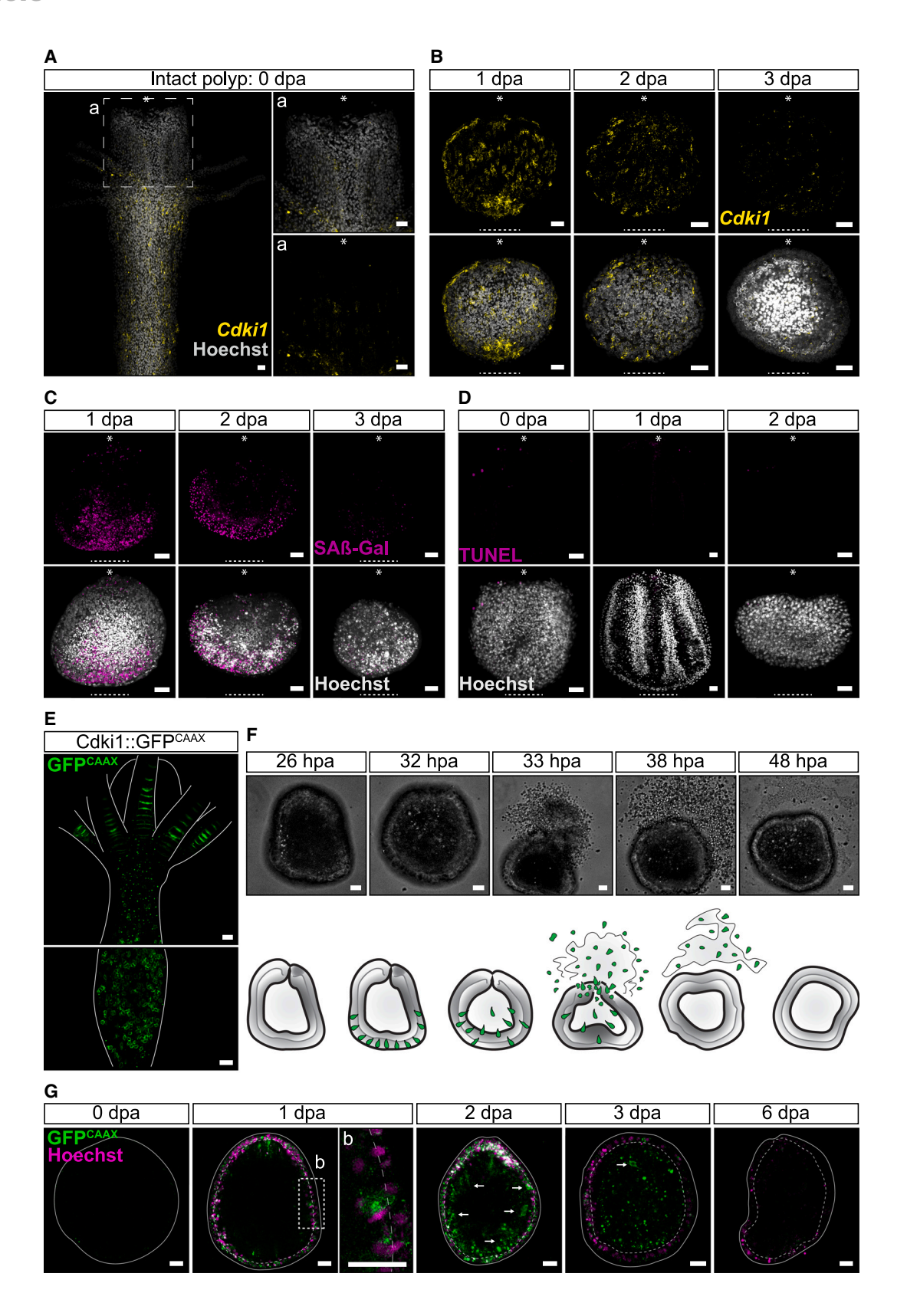
SASP) that promotes reprogramming of neighboring somatic cells. This would, in turn, produce stem cells that could initiate a regenerative process.

Following this line of reasoning, we looked for indicators of senescence in regenerating hypostomes. Cell-cycle regulators such as p21 (encoded by CDKN1A) and p16 (encoded by CDKN2A) are known senescence markers in mammals.<sup>21</sup> The Hydractinia genome encodes three CDKN1A-like genes

(Figures S4 and S5) but no CDKN2A, the latter being vertebrate specific. Our phylogeny could not resolve orthology between cnidarian and bilaterian CDKN1A proteins, suggesting that the Hydractinia genes were paralogs. Therefore, we called the three Hydractinia CDKN1A-like genes Cyclin-dependent kinase inhibitor 1 (Cdki1; HyS0010.253), Cdki2 (HyS0001.744), and Cdki3 (HyS0029.124), respectively. Single-molecule fluorescence mRNA in situ hybridization showed that the three genes were

## **Cell Reports Article**





(legend on next page)



expressed in some cells along the body column (Figures 3A and S5A) but that only Cdki1 was upregulated at the cut side of isolated hypostomes around 1 dpa (Figure 3B), being nearly undetectable in intact hypostomes (Figure 3A) and in the blastema of regenerating polyps (Figure S6). Expression patterns of Cdki2 and Cdki3 did not visibly change following injury. An additional senescence indicator is senescence-associated β-galactosidase (SAβ-Gal) activity.<sup>21</sup> Using SPiDER-βGal, a cell-permeable fluorescent  $\beta$ -Gal probe, we found high SA $\beta$ -Gal activity around the injury site of hypostomes, concomitant with Cdki1 expression (Figures 3C and S6A). The above signals reached a peak around 1 dpa and vanished 2-3 dpa, indicating a transient, short-term senescence episode at the injury site post amputation.

In the closely related chidarian Hydra, it has been shown that bisection induces apoptosis in i-cells, with these dying cells emitting a Wnt3 signal that drives proliferation and head regeneration.<sup>22</sup> However, in regenerating Hydractinia hypostomes, no evidence for apoptosis was found using TUNEL staining (Figures 3D, S4B, and S4C), suggesting that senescenceinduced regeneration in the absence of stem cells is distinct from apoptosis-induced repair where i-cells are present.

Given that senescent cells do not spontaneously die or normally exit senescence, the disappearance of senescence markers between the second and third dpa prompted us to investigate their fates. For this, we generated a Cdki1 transgenic reporter animal that expressed membrane GFP<sup>CAAX</sup> under the Cdki1 genomic control elements.  $\textit{GFP}^{\textit{CAAX}}$  fluorescence in transgenic animals faithfully recapitulated Cdki1 mRNA expression (Figure 3E), being upregulated at the injury site 1 dpa (Figures S5B-S5C). We amputated hypostomes from these animals and subjected them to in vivo time-lapse imaging (Figures 3F and S5D; Video S1). Strikingly, these experiments showed that epidermal senescent cells translocate to the gastrodermal tissue (Figure 3G) and are then expelled, probably through the mouth, by regenerating hypostomes between 30 and 40 h post amputation (hpa; Figures 3F-3G and S5C-S5D), consistent with the disappearance of senescence markers (Figure 3C). Therefore, whole-body regeneration from isolated hypostomes is accompanied by a short senescence period around 1 dpa, loss of tissue polarity within 3 dpa, a burst of proliferation around 3-4 dpa, and secondary i-cell appearance 6 dpa (Figure 4A). The process is completed by the re-establishment of tissue polarity, elongation, and morphogenesis.

#### Senescence signaling is required and sufficient to induce reprogramming

To identify a functional link between the short period of senescence and the subsequent reprogramming of somatic cells, we used navitoclax, a senolytic drug,<sup>23</sup> to inhibit senescence and study the effect of this manipulation on somatic cell reprogramming and secondary i-cell appearance. We exposed freshly amputated hypostomes to 1 µM navitoclax in seawater and followed them over 6 dpa. We found that navitoclax at this concentration inhibited senescence marker upregulation for the duration of treatment (Figures 4B and S7A). Furthermore, no secondary i-cells appeared in treated hypostomes at 6 dpa (Figure 4C). We repeated the experiments with rapamycin, an mTOR inhibitor, which yielded similar results (Figure S7B-S7C).

To further address the requirement of senescence to reprogramming, and exclude an unspecific effect of senolytic drugs, we used CRISPR-Cas9 to mutate the Cdki1 gene (Figure S8A). Three short guide RNAs (sgRNAs) targeting the nuclear localization signal (NLS) and proliferating cell nuclear antigen (PCNA)-interacting domain of Cdki1 were designed and injected with recombinant Cas9 into fertilized eggs.24 G0 embryos were allowed to develop into larvae, metamorphose, and grow to the young colony stage. They were then screened for mutations by genomic PCR and sequencing. Confirmed mosaic mutants were grown to sexual maturity and crossed with wild-type animals. Heterozygous G1 animals were identified by PCR and sequencing, grown to sexual maturity, and interbred to give rise to G2 homozygous knockout (KO) animals (Figure S8A). These animals developed normally to the larval stage, metamorphosed, and grew to apparently normal colonies that were able to regenerate amputated heads similar to those seen in wild-type animals (Figure S8B). However, EdU analysis revealed that Cdki1 KO animals had an abnormal, broader distribution of cycling cells, consistent with the loss of a cell-cycle regulator (p < 0.0001, n = 20; Figures S8C-S8D; Data S2).

We amputated hypostomes from Cdki1 KO animals and analyzed their behavior. We found that the absence of functional Cdki1 resulted in the loss of the senescence response at 1 dpa (Figure 4B) and the absence of secondary i-cells at 6 dpa (Figure 4C). With the lack of i-cells, the KO hypostomes had not regenerated within 20 dpa (Figure 4D), remaining as amorphous tissue lumps that eventually died of starvation. Therefore, short senescence signaling is essential for reprogramming.

#### Figure 3. Senescence markers are transiently upregulated 1 dpa

(A) Cdki1 mRNA SABER-FISH of an intact Hydractinia polyp. Low levels of Cdki1 mRNA are present in the hypostome.

(B) Cdki1 mRNA SABER-FISH of amputated hypostomes 1, 2, and 3 dpa. Cdki1 mRNA is upregulated at the site of injury (dashed line) at 1 dpa and dissipates 3 dpa. Asterisks indicate the oral pole pre-amputation.

(C) SPiDER-βGal staining of amputated hypostomes 1, 2, and 3 dpa. βGal activity resembles Cdki1 mRNA expression pattern at the site of injury (dashed line). Asterisks indicate the oral pole pre-amputation.

- (D) Absence of apoptosis (TUNEL) at the site of injury (dashed line). Asterisks indicate the oral pole pre-amputation.
- (E) In vivo imaging of an intact Cdki1:GFP<sup>CAAX</sup> transgenic reporter animal.
- (F) Time-lapse imaging (extracted from Video S1) of an amputated Cdki1:GFP<sup>CAAX</sup> reporter hypostome at 26, 32, 33, 38, and 48 hpa. Interpretation of the images
- (G) Time-lapse imaging of amputated hypostomes from a Cdki1:GFP<sup>CAAX</sup> reporter animal showing the migration of senescent cells from the epidermis to the gastrodermis (arrows). No Cdki1:GFPCAAX cells are present 6 dpa. Scale bars: 20 μm. See also Figures S4-S6.



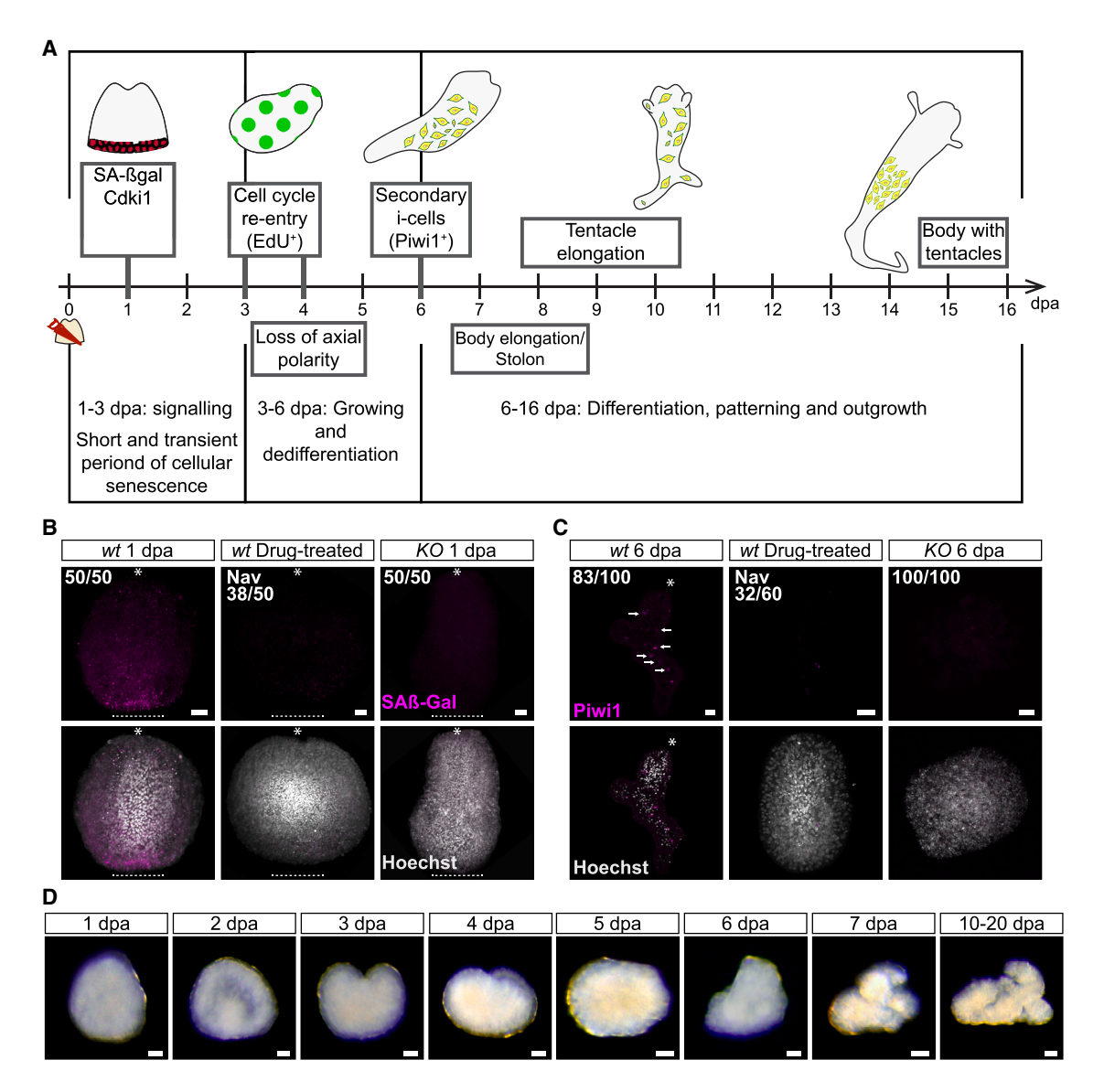


Figure 4. Transient senescence 1 dpa is required for somatic cell reprogramming

- (A) Diagrammatic illustration of the major events accompanying whole-body regeneration from amputated hypostomes.
- (B) Hypostomes amputated from both Navitoclax-treated wild-type and Cdki1 KO animals do not develop cellular senescence at the site of injury 1 dpa (dashed line). Asterisks indicate the oral pole pre-amputation.
- (C) Hypostomes amputated from Navitoclax-treated and Cdki1 KO animals do not develop Piwi1+ cells (arrows) at 6 dpa. Asterisks indicate the oral pole.
- (D) Amputated hypostomes from Cdki1 KO animals do not regenerate within 20 dpa. Scale bars: 20 µm.

See also Figures S7 and S8.

Finally, we tested the ability of ectopic senescence to induce reprogramming in this specific context. To induce senescence, we employed an optogenetic approach using the Opto-SOS genetic cassette.<sup>25</sup> Cells carrying this construct respond to blue light by overactivation of the Ras pathway (Figure 5A), and overactivation of Ras is known to induce senescence.<sup>26</sup> We generated transgenic mosaic animals that carried the Opto-SOS construct, fused to mScarlet. Hypostomes were amputated and exposed to blue light for 12 hpa (Figure 5B); we then observed the events accompanying their regeneration. As expected, we found that exposure to blue light (which

caused Ras pathway activation through the Opto-SOS construct) induced enhanced SAβ-Gal activity (Figures 5C and 5D), and secondary i-cells appeared 5 dpa (Figure S9A) as opposed to 6 dpa in animals kept in the dark; animals exposed to blue light grew faster than control ones (Figure S9A). At 6 dpa, the number of secondary i-cells was significantly enhanced in animals exposed to blue light compared with those kept in the dark (p < 0.0001, n = 44; Figures 5E and 5F; Data S2). To confirm the involvement of Cdki1-mediated senescence signaling and exclude a non-specific effect of the Opto-SOS construct, we treated hypostomes with Navitoclax.



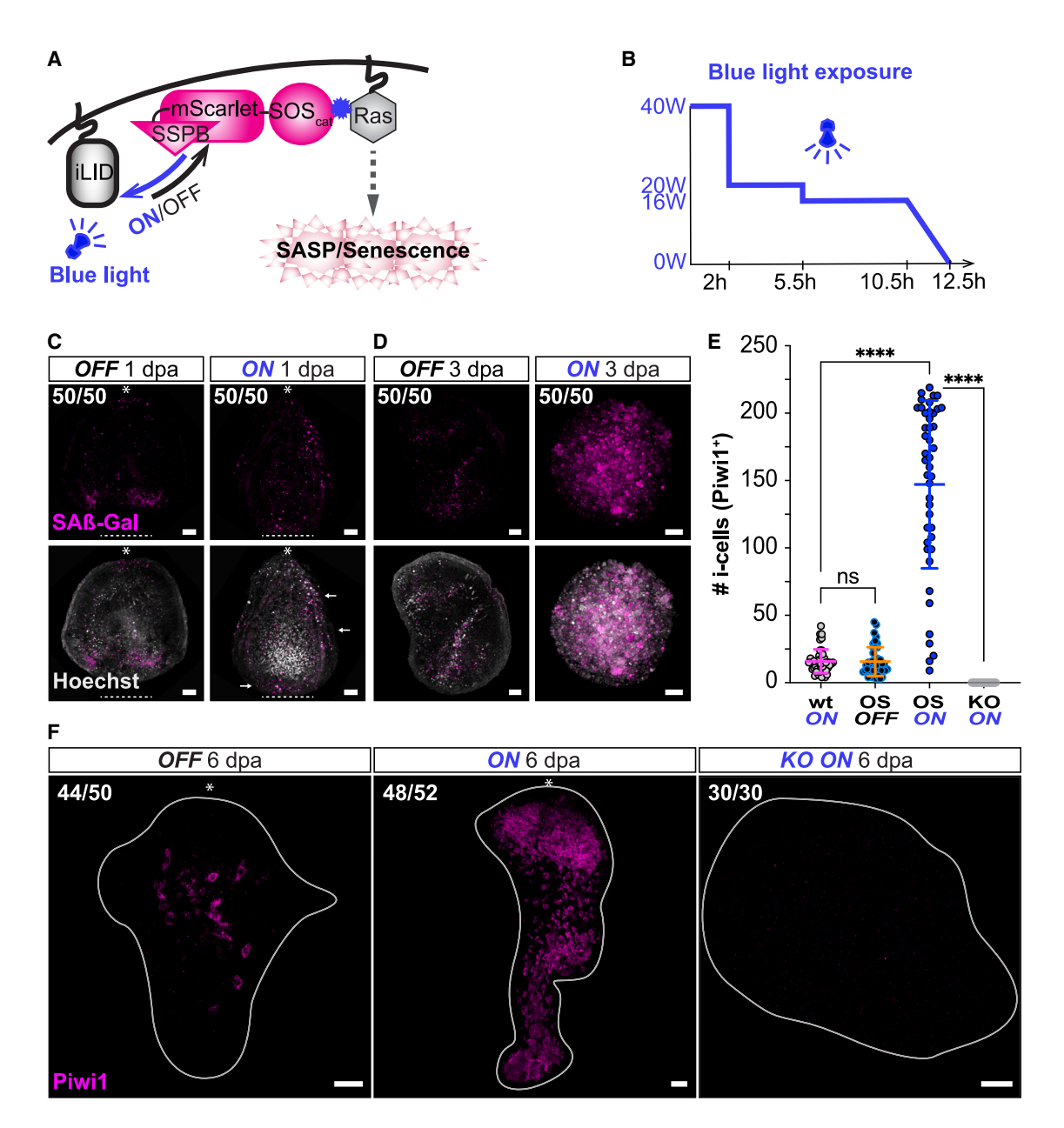


Figure 5. An optogenetic approach for ectopic induction of senescence during regeneration results in increased numbers of secondary

- (A) A diagrammatic representation of the optogenetic activation of the Ras pathway when exposed to blue light.
- (B) Blue light exposure pattern during the experiments.
- (C) Ectopic senescence outside the site of injury at 1 dpa (dashed line) under blue light exposure. Asterisks indicate the oral pole pre-amputation.
- (D) Enhanced cellular senescence 3 dpa under blue light exposure.
- (E) Quantification of the number of secondary i-cells at 6 dpa (p < 0.0001; wild type [WT] and OptoSOS [OS] n = 44; KO n = 30). Amputated hypostomes were incubated during 1 dpa under four different conditions: WT under blue light exposure (WT ON), OS under darkness (OS OFF), OS under blue light exposure (OS ON), and Cdki1 KO OptoSOS under blue light exposure (KO ON).
- (F) Supernumerary secondary i-cells at 6 dpa under blue light exposure. Scale bars: 20  $\mu m$ . See also Figure S9.

This caused a reduction in the number of secondary i-cells (Figures S9B-S9C). Finally, we generated Cdki1 KO animals that carried the Opto-SOS construct. However, after exposing them to blue light (Figures 5E and 5F), no i-cells were identified in their tissues. Taken together, a signal emitted by senescent cells that are transiently present following injury is essential and sufficient to induce the reprogramming of somatic cells to stemness in amputated hypostomes.

#### **Article**



#### **DISCUSSION**

Animal somatic cells face contradictory requirements during the life history of individuals. On the one hand, cell fate stability is needed to maintain structural integrity and prevent malignancy, while, on the other hand, stably differentiated cells prevent regeneration. Extant animals appear to deal with this problem using a spectrum of strategies. Morphologically simple animals such as cnidarians possess high cellular plasticity and regenerative powers. They can tolerate the presence of unstable cells because their structural organization facilitates the shedding of unwanted cells (Figures 3F and 3G). By contrast, morphologically complex bilaterians such as mammals cannot afford to harbor developmentally plastic cells due to malignancy risk and the necessity to maintain complex structures. The results presented here are consistent with the notion that senescence signaling is one of the factors that mediate cellular plasticity. 13,27 Recently, studies using salamanders have shown a similar role for senescence in limb regeneration.<sup>28,29</sup> However, the ability to respond to a senescence signal by inducing reprogramming has not been highly conserved across lineages during metazoan evolution.

A rudimentary response to senescence signals by increased plasticity is still present in modern mammals. This has been shown in mouse liver cells<sup>18</sup> and skeletal muscles<sup>30</sup> and by the discovery that a senescent environment facilitates reprogramming by OSKM factors.31 Finally, embryonic and induced pluripotent stem cells maintain pluripotency when grown on a feeder layer consisting of senescent fibroblasts.<sup>32</sup> However, except for urodele amphibians, 19 tetrapod vertebrates have poor regenerative ability and do not respond to a senescence signal as effectively as *Hydractinia*.

We suggest that senescence is an ancient mechanism, instructing cells adjacent to an injury site to prepare for a regenerative event. We also speculate that other consequences of senescence that have been observed in mammals, such as long-term retention and accumulation of senescent cells, aging, chronic inflammation, and cancer, are side effects that evolved later in the evolution of these lineages, perhaps as a consequence of the increase in cell fate stability and morphological complexity. Understanding the senescent environment and its role in cellular plasticity could pave the way for new treatments to enhance regeneration in poorly regenerating mammals.

#### **Limitations of the study**

Our study provides strong evidence for a role for senescence signaling in cellular reprograming in cnidarians. While similar phenomena have been observed by others in other animals, the degree to which components of the senescence signaling pathway are evolutionarily conserved across phyla is, at present, unclear. Markers for cellular senescence are not universal, and no definitive marker for senescence has been identified. Moreover, the existence of different senescence "types" has been proposed.<sup>33</sup> Finally, we have not been able to show that secondary i-cells are pluripotent, as are primary i-cells.

#### **STAR**\*METHODS

Detailed methods are provided in the online version of this paper and include the following:

- KEY RESOURCES TABLE
- RESOURCE AVAILABILITY
  - Lead contact
  - Materials availability
  - Data and code availability
- EXPERIMENTAL MODEL AND STUDY PARTICIPANT DE-**TAILS** 
  - Animals
- METHOD DETAILS
  - Hypostome isolation
  - SpiDER-Gal staining
  - RNA isolation from hypostome tissue
  - O Differential expression and candidate gene enrichment
  - O Transgenic animals
  - CRISPR-Cas9 knockout
  - Single polyp genomic DNA extraction
  - Genotyping CRISPR-Cas9 knockouts
  - SABER-FISH
  - Optogenetics
  - Drug treatments
  - Cellular staining
  - EdU staining
  - TUNEL labeling
  - Imaging
  - Phylogenetic analysis
- QUANTIFICATION AND STATISTICAL ANALYSIS

#### SUPPLEMENTAL INFORMATION

Supplemental information can be found online at https://doi.org/10.1016/j. celrep.2023.112687.

#### **ACKNOWLEDGMENTS**

We thank all members of the Frank lab for discussions and advice. The NIH Intramural Sequencing Center (NISC) is kindly acknowledged for generating the RNA sequence data. Confocal images were taken at the Centre for Microscopy and Imaging Core Facility at University of Galway. U.F. is a Wellcome Trust Investigator in Science (grant no. 210722/Z/18/Z), and work in the Frank lab is also funded by the NSF EDGE program (grant no. 1923259). M.S.-S. is a Human Frontier Science Program Long-Term Postdoctoral Fellow (grant no. LT000756/2020-L), G.K. is an Irish Research Council postdoctoral fellow (project ID GOIPD/2020/149). H.R.H. is a doctoral student at the Science Foundation Ireland Centre for Research Training in Genomic Data Science (grant no. 18/CRT/6214). A.D.B. is funded by the Intramural Research Program of the National Human Genome Research Institute, National Institutes of Health (project no. ZIA HG000140).

#### **AUTHOR CONTRIBUTION**

M.S.-S. and U.F. conceptualized the study. M.S.-S. performed experiments. G.K. performed phylogeny and TUNEL assays. H.R.H. and F. analyzed differential gene expression (DGE) data. A.D.B. supervised the generation of RNA sequencing (RNA-seq) data and making these data publicly available as described in the data and code availability section. M.S.-S. and U.F. designed the experiments, analyzed data, and wrote the paper. All authors commented on and approved the manuscript.

#### **DECLARATION OF INTERESTS**

The authors declare no competing interests.





Received: August 4, 2022 Revised: May 11, 2023 Accepted: June 7, 2023 Published: June 30, 2023

#### REFERENCES

- 1. Bely, A.E., and Nyberg, K.G. (2010). Evolution of animal regeneration: reemergence of a field. Trends Ecol. Evol. 25, 161-170. https://doi.org/10. 1016/i.tree.2009.08.005.
- 2. Tanaka, E.M., and Reddien, P.W. (2011). The cellular basis for animal regeneration. Dev. Cell 21, 172-185. https://doi.org/10.1016/j.devcel.
- 3. Slack, J.M. (2017). Animal regeneration: ancestral character or evolutionary novelty? EMBO Rep. 18, 1497-1508. https://doi.org/10.15252/ embr.201643795
- 4. Sánchez Alvarado, A., and Yamanaka, S. (2014). Rethinking differentiation: stem cells, regeneration, and plasticity. Cell 157, 110-119. https:// doi.org/10.1016/j.cell.2014.02.041.
- 5. Bradshaw, B., Thompson, K., and Frank, U. (2015). Distinct mechanisms underlie oral vs aboral regeneration in the cnidarian Hydractinia echinata. Elife 4, e05506. https://doi.org/10.7554/eLife.05506.
- 6. Varley, Á., Horkan, H.R., McMahon, E.T., Krasovec, G., and Frank, U. (2023). Pluripotent, germ cell competent adult stem cells undelie cnidarina regenerative ability and clonal growth. Curr. Biol. 33, 1883-1892.e3. https://doi.org/10.1016/j.cub.2023.03.039.
- 7. Gahan, J.M., Bradshaw, B., Flici, H., and Frank, U. (2016). The interstitial stem cells in Hydractinia and their role in regeneration. Curr. Opin. Genet. Dev. 40, 65-73. https://doi.org/10.1016/j.gde.2016.06.006.
- 8. DuBuc, T.Q., Schnitzler, C.E., Chrysostomou, E., McMahon, E.T., Febrimarsa Gahan, J.M., Gahan, J.M., Buggie, T., Gornik, S.G., Hanley, S., Barreira, S.N., et al. (2020). Transcription factor AP2 controls cnidarian germ cell induction. Science 367, 757-762. https://doi.org/10.1126/science.
- 9. Subach, F.V., Subach, O.M., Gundorov, I.S., Morozova, K.S., Piatkevich, K.D., Cuervo, A.M., and Verkhusha, V.V. (2009). Monomeric fluorescent timers that change color from blue to red report on cellular trafficking. Nat. Chem. Biol. 5, 118-126. https://doi.org/10.1038/nchembio.138.
- 10. Plickert, G., Jacoby, V., Frank, U., Müller, W.A., and Mokady, O. (2006). Wnt signaling in hydroid development: formation of the primary body axis in embryogenesis and its subsequent patterning. Dev. Biol. 298, 368-378
- 11. Duffy, D.J., Plickert, G., Künzel, T., Tilmann, W., and Frank, U. (2010). Wnt signaling promotes oral but suppresses aboral structures in Hydractinia metamorphosis and regeneration. Development 137, 3057-3066. https://doi.org/10.1242/dev.046631.
- 12. Avelar, R.A., Ortega, J.G., Tacutu, R., Tyler, E.J., Bennett, D., Binetti, P., Budovsky, A., Chatsirisupachai, K., Johnson, E., Murray, A., et al. (2020). A multidimensional systems biology analysis of cellular senescence in aging and disease. Genome Biol. 21, 91. https://doi.org/10. 1186/s13059-020-01990-9.
- 13. Rhinn, M., Ritschka, B., and Keyes, W.M. (2019). Cellular senescence in development, regeneration and disease. Development 146, dev151837. https://doi.org/10.1242/dev.151837.
- 14. Roy, A.L., Sierra, F., Howcroft, K., Singer, D.S., Sharpless, N., Hodes, R.J., Wilder, E.L., and Anderson, J.M. (2020). A blueprint for characterizing senescence. Cell 183, 1143-1146. https://doi.org/10.1016/j.cell.2020. 10.032.
- 15. Krtolica, A., Parrinello, S., Lockett, S., Desprez, P.-Y., and Campisi, J. (2001). Senescent fibroblasts promote epithelial cell growth and tumorigenesis: a link between cancer and aging. Proc. Natl. Acad. Sci. USAUSA 98, 12072-12077. https://doi.org/10.1073/pnas.211053698.
- 16. Paramos-de-Carvalho, D., Jacinto, A., and Saúde, L. (2021). The right time for senescence. Elife 10, e72449. https://doi.org/10.7554/eLife.72449.

- 17. Baker, D.J., Wijshake, T., Tchkonia, T., LeBrasseur, N.K., Childs, B.G., van de Sluis, B., Kirkland, J.L., and van Deursen, J.M. (2011). Clearance of p16lnk4a-positive senescent cells delays ageing-associated disorders. Nature 479, 232-236. https://doi.org/10.1038/nature10600.
- 18. Ritschka, B., Storer, M., Mas, A., Heinzmann, F., Ortells, M.C., Morton, J.P., Sansom, O.J., Zender, L., and Keyes, W.M. (2017). The senescence-associated secretory phenotype induces cellular plasticity and tissue regeneration. Genes Dev. 31, 172-183. https://doi.org/10.1101/gad. 290635.116.
- 19. Walters, H.E., and Yun, M.H. (2020). Rising from the ashes: cellular senescence in regeneration. Curr. Opin. Genet. Dev. 64, 94-100. https://doi.org/ 10.1016/j.gde.2020.06.002.
- 20. Da Silva-Álvarez, S., Guerra-Varela, J., Sobrido-Cameán, D., Quelle, A., Barreiro-Iglesias, A., Sánchez, L., and Collado, M. (2020). Cell senescence contributes to tissue regeneration in zebrafish. Aging Cell 19, e13052. https://doi.org/10.1111/acel.13052.
- 21. Hernandez-Segura, A., Nehme, J., and Demaria, M. (2018). Hallmarks of cellular senescence. Trends Cell Biol. 28, 436-453. https://doi.org/10. 1016/i.tcb.2018.02.001.
- 22. Chera, S., Ghila, L., Dobretz, K., Wenger, Y., Bauer, C., Buzgariu, W., Martinou, J.-C., and Galliot, B. (2009). Apoptotic cells provide an unexpected source of Wnt3 signaling to drive Hydra head regeneration. Dev. Cell 17, 279-289
- 23. Chang, J., Wang, Y., Shao, L., Laberge, R.M., Demaria, M., Campisi, J., Janakiraman, K., Sharpless, N.E., Ding, S., Feng, W., et al. (2016). Clearance of senescent cells by ABT263 rejuvenates aged hematopoietic stem cells in mice. Nat. Med. 22, 78-83. https://doi.org/10.1038/nm.4010.
- 24. Gahan, J.M., Schnitzler, C.E., DuBuc, T.Q., Doonan, L.B., Kanska, J., Gornik, S.G., Barreira, S., Thompson, K., Schiffer, P., Baxevanis, A.D., and Frank, U. (2017). Functional studies on the role of Notch signaling in Hydractinia development. Dev. Biol. 428, 224-231. https://doi.org/10.1016/ j.ydbio.2017.06.006.
- 25. Johnson, H.E., Goyal, Y., Pannucci, N.L., Schüpbach, T., Shvartsman, S.Y., and Toettcher, J.E. (2017). The spatiotemporal limits of developmental erk signaling. Dev. Cell 40, 185-192. https://doi.org/10.1016/j.devcel.2016.12.002.
- 26. Serrano, M., Lin, A.W., McCurrach, M.E., Beach, D., and Lowe, S.W. (1997). Oncogenic ras provokes premature cell senescence associated with accumulation of p53 and p16 INK4a</sup&gt. Cell 88, 593-602. https://doi.org/10.1016/S0092-8674(00)81902-9.
- 27. Ring, N.A.R., Valdivieso, K., Grillari, J., Redl, H., and Ogrodnik, M. (2022). The role of senescence in cellular plasticity: lessons from regeneration and development and implications for age-related diseases. Dev. Cell 57, 1083-1101. https://doi.org/10.1016/j.devcel.2022.04.005.
- 28. Yu, Q., Walters, H.E., Pasquini, G., Singh, S.P., León-Periñán, D., Petzold, A., Kesavan, P., Subiran, C., Garteizgogeascoa, I., Knapp, D., et al. (2022). Cellular senescence modulates progenitor cell expansion during axolotl limb regeneration. Preprint at bioRxiv, 2022-2009. https://doi.org/10. 1101/2022.09.01.506196.
- 29. Walters, H.E., Troyanovskiy, K., and Yun, M.H. (2022). Senescent cells enhance newt limb regeneration by promoting muscle dedifferentiation. Preprint at bioRxiv, 2022-2009. https://doi.org/10.1101/2022.09.01. 506186
- 30. Chiche, A., Le Roux, I., von Joest, M., Sakai, H., Aguín, S.B., Cazin, C., Salam, R., Fiette, L., Alegria, O., Flamant, P., et al. (2017). Injury-induced senescence enables in vivo reprogramming in skeletal muscle. Cell Stem Cell 20, 407-414.e4. https://doi.org/10.1016/j.stem.2016.11.020.
- 31. Mosteiro, L., Pantoja, C., Alcazar, N., Marión, R.M., Chondronasiou, D., Rovira, M., Fernandez-Marcos, P.J., Muñoz-Martin, M., Blanco-Aparicio, C., Pastor, J., et al. (2016). Tissue damage and senescence provide critical signals for cellular reprogramming in vivo. Science 354, aaf4445. https:// doi.org/10.1126/science.aaf4445.

#### **Article**



- 32. Takahashi, K., and Yamanaka, S. (2006). Induction of pluripotent stem cells from mouse embryonic and adult fibroblast cultures by defined factors. Cell 126, 663-676.
- 33. Varela-Eirín, M., and Demaria, M. (2022). Cellular senescence. Curr. Biol. 32, R448-R452. https://doi.org/10.1016/j.cub.2022.04.003.
- 34. Kishi, J.Y., Lapan, S.W., Beliveau, B.J., West, E.R., Zhu, A., Sasaki, H.M., Saka, S.K., Wang, Y., Cepko, C.L., and Yin, P. (2019). SABER amplifies FISH: enhanced multiplexed imaging of RNA and DNA in cells and tissues. Nat. Methods 16, 533-544. https://doi.org/10.1038/s41592-019-0404-0.
- 35. Frank, U., Nicotra, M.L., and Schnitzler, C.E. (2020). The colonial cnidarian Hydractinia. EvoDevo 11, 7. https://doi.org/10.1186/s13227-020-
- 36. Kim, D., Langmead, B., and Salzberg, S.L. (2015). HISAT: a fast spliced aligner with low memory requirements. Nat. Methods 12, 357-360. https://doi.org/10.1038/nmeth.3317.
- 37. Liao, Y., Smyth, G.K., and Shi, W. (2014). featureCounts: an efficient general purpose program for assigning sequence reads to genomic features.

- Bioinformatics 30, 923-930. https://doi.org/10.1093/bioinformatics/ btt656
- 38. Love, M.I., Huber, W., and Anders, S. (2014). Moderated estimation of fold change and dispersion for RNA-seq data with DESeq2. Genome Biol.
- 39. Künzel, T., Heiermann, R., Frank, U., Müller, W., Tilmann, W., Bause, M., Nonn, A., Helling, M., Schwarz, R.S., and Plickert, G. (2010). Migration and differentiation potential of stem cells in the cnidarian Hydractinia analysed in GFP-transgenic animals and chimeras. Dev. Biol. 348, 120–129.
- 40. Chrysostomou, E., Flici, H., Gornik, S.G., Salinas-Saavedra, M., Gahan, J.M., McMahon, E.T., Thompson, K., Hanley, S., Kilcoyne, M., Schnitzler, C.E., et al. (2022). A cellular and molecular analysis of SoxB-driven neurogenesis in a cnidarian. Elife 11, e78793. https://doi.org/10.7554/eLife. 78793.
- 41. Moreno-Mateos, M.A., Vejnar, C.E., Beaudoin, J.D., Fernandez, J.P., Mis, E.K., Khokha, M.K., and Giraldez, A.J. (2015). CRISPRscan: designing highly efficient sgRNAs for CRISPR-Cas9 targeting in vivo. Nat. Methods 12, 982-988. https://doi.org/10.1038/nmeth.3543.





#### **STAR**\***METHODS**

#### **KEY RESOURCES TABLE**

REAGENT or RESOURCE	SOURCE	IDENTIFIER
Antibodies		
Rabbit anti-Piwi1	In house (DuBuc et al. <sup>8</sup> )	N/A
Chicken polyclonal RFP antibody	Synaptic Systems	Cat#409 006; RRID: AB_2725776
Chemicals, peptides, and recombinant protein	ns .	
Rapamycin	Sigma-Aldrich	553210; CAS: 53123-88-9
Navitoclax (Synonyms: ABT-263)	MedChemExpress	HY-10087; CAS: 923564-51-6
Critical commercial assays		
Click-iT <sup>TM</sup> EdU Cell Proliferation Kit for Imaging, Alexa Fluor <sup>TM</sup> 488 dye	Invitrogen	C10337
TM red In Situ Cell Death Detection Kit	Roche	12156792910
SpiDER-Gal	Dojindo Inc.	SG03-10
Deposited data		
Raw and analyzed data	This paper	NCBI Sequence Read Archive (SRA) BioProject PRJNA807936; BioProject PRJNA824817
Hydractinia symbiolongicarpus genome	NIH National Human Genome Research Institute	https://research.nhgri.nih.gov/hydractinia/ RRID:SCR_022602
Experimental models: Organisms/strains		
Hydractinia symbiolongicarpus	N/A	RRID:SCR_022602
Oligonucleotides		
PER hairpin (SABER-FISH) h.30.30.ip AAATACTCTCGGGCCTTTTGGCC CGAGAGTATTTGAGAGTATT/3InvdT/	Kishi et al. <sup>34</sup>	IDT, HPLC-purified
PER hairpin (SABER-FISH) h.27.27.ip ACATCATCATGGGCCTTTTGGCCC ATGATGATGTATGATGATGATGATGATGATGATGATGATG	Kishi et al. <sup>34</sup>	IDT, HPLC-purified
Fluor Oligo (SABER-FISH) 30*.633 /5ATTO633N/ TTGAGAGTATTTGAGAGTATTT	Kishi et al. <sup>34</sup>	IDT, HPLC-purified
Additional oligonucleotides	This paper, Table S1	N/A
Recombinant DNA		
Plasmid: Fast-FT-P2A-GFP <sup>CAAX</sup>	This paper	N/A
Plasmid: Cdki1:GFP <sup>CAAX</sup>	This paper	N/A
Plasmid: βtub:OptoSos	This paper	N/A
Software and algorithms		
Geneious 8.0.3	www.geneious.com	N/A
ImageJ/Fiji	www.imagej.net	N/A
GraphPad Prism 8	www.graphpad.com	N/A
MAFFT	www.ebi.ac.uk/Tools/msa/mafft/	N/A
GBlocks 0.91b	http://molevol.cmima.csic.es/ castresana/Gblocks.html	N/A
PhyML	http://www.atgc-montpellier.fr/phyml/	N/A
MrBayes	https://nbisweden.github.io/MrBayes/	N/A

(Continued on next page)

#### **Article**



Continued			
REAGENT or RESOURCE	SOURCE	IDENTIFIER	
Trim Galore	https://www.bioinformatics. babraham.ac.uk/projects/trim_galore/	N/A	
HISAT2	http://daehwankimlab.github.io/hisat2/	N/A	
Subread	http://subread.sourceforge.net	N/A	
DESeq2	https://github.com/mikelove/DESeq2	N/A	
R	https://www.r-project.org	N/A	
EggNOG-Mapper V5.0	http://eggnog-mapper.embl.de	N/A	
ClusterProfiler 4.0	https://guangchuangyu.github.io/software/clusterProfiler/	N/A	

#### **RESOURCE AVAILABILITY**

#### Lead contact

Further information and requests for resources and reagents should be directed to and will be fulfilled by the lead contact, Uri Frank (uri.frank@universityofgalway.ie).

#### **Materials availability**

This study did not generate new unique reagents.

#### **Data and code availability**

- The Hydractinia symbiolongicarpus genome is available in the Hydractinia Genome Project Portal through the NIH National Human Genome Research Institute of the National Institutes of Health (https://research.nhgri.nih.gov/hydractinia/) and at NCBI BioProject PRJNA807936, BioSample SAMN26021137. Data corresponding to RNA-seq have been deposited under BioProject PRJNA824817.
- Bioinformatics scripts are available at https://github.com/UriFrankLab/Hsym\_Hypostome\_DiffExpr.
- Any additional information required to reanalyze the data reported in this paper is available from the lead contact upon request.

#### **EXPERIMENTAL MODEL AND STUDY PARTICIPANT DETAILS**

#### **Animals**

Adult Hydractinia symbiolongicarpus colonies were maintained as described. 35 Female and male colonies were grown on glass slides kept in artificial seawater (ASW) at 19-22°C. Animals were fed four times per week with Artemia nauplii, and once a week with pureed oysters. To induce scheduled spawning, we kept the animals in a constant 14:10 light:dark cycle, where females and males spawn 1.5 h after exposure to light.

#### **METHOD DETAILS**

#### **Hypostome** isolation

One day starved adult H. symbiolongicarpus colonies were anesthetized in 4% MgCl<sub>2</sub> (in 50% distilled water/50% filtered seawater). Polyps were dissected from the colony and decapitated. Hypostomes were isolated by removing the tentacles. Hypostomes were transferred to a glass Petri dish with freshly 0.2 µm filtered seawater and incubated at 22.4-23°C with constant reciprocal shaking in a temperature-controlled incubator. 0.2 µm filtered sea water was changed every two days.

#### **SpiDER-Gal staining**

Hypostomes were collected and fixed in 0.2% glutaraldehyde (stock: 25%, Sigma-Aldrich; G5882), 4% paraformaldehyde (stock: 16%, Alfa Aesar; 43368) in filtered seawater for 2 min. Then, the fixative was replaced by 4% paraformaldehyde in filtered seawater and samples were incubated for 40 min. Samples were rinsed twice with seawater (3 min each) and proceed as per manufacturer's indications. Samples were equilibrated with 1x McIlvaine buffer, pH 6.0 (5x: 0.1 M citric acid solution, 0.2 M sodium phosphate solution) for 5 min. Then, samples were incubated with 1:500 SpiDER-Gal (1 mM; SG03-10, Dojindo Inc.) in 1x McIlvaine buffer for 1 h at RT. Samples were washed once with 1X PBST (0.3% Triton X-100 in 1X PBS) for 5 min, stained with Hoechst (20 mg/mL) 1:2000 in 1X PBST for 15 min, washed with 1X PBST, and mounted for imaging. Live animal staining with SpiDER-Gal was carried out in seawater.





#### RNA isolation from hypostome tissue

Total RNA was extracted from isolated hypostomes collected from wild type H. symbiolongicarpus strain 291-10. Samples consisted of three replicates of 220 hypostomes each at 0-, 1-, 3-, and 6-days post amputation (dpa). RNA was isolated using Direct-zol RNA MiniPrep kit (Zymo Research; R2050) per the manufacturer's instructions. The eluted RNA was quantified using NanoDrop and the quality was checked using agarose-formaldehyde gel electrophoresis. After RNA isolation, samples were shipped to the NIH Intramural Sequencing Center (NISC) for further processing and sequencing. RNA was amplified with the Ovation RNA-Seq System V2 kit, and sequencing libraries were made with Illumina TruSeq Stranded mRNA Library Prep Kit. Libraries were sequenced on one lane of Illumina NovaSeg 6000 (2x151 bp), generating between 87 and 137 million reads per sample (average 112 million reads). Only two replicates for 6 dpa were sequenced.

#### Differential expression and candidate gene enrichment

Raw reads were trimmed and aligned to the reference genome using Trim Galore https://www.bioinformatics.babraham.ac.uk/ projects/trim\_galore/and HISAT2, 36 respectively. A count matrix of mapped reads per genomic feature was generated using Subread featureCounts<sup>37</sup> and converted into a DESeqDataSet. This dataset was used as an input to DESeq2<sup>38</sup> in order to generate a list of differentially expressed genes for each time point compared to the preceding time point. We used CellAgeDB to obtain a list of candidate genes involved in cellular senescence. We identified Hydractinia homologs of these genes from the genome by reciprocal BLAST search using query sequences obtained from UniProt. We searched for these homologs in our list of differentially expressed genes in all time points and plotted a heatmap of differentially expressed genes, with the following parameters: Scale Type = None, Clustering Method = Average Linkage and Distance Measurement Method = Pearson.

#### **Transgenic animals**

The generation of stable transgenic reporter animals was carried out as previously described.<sup>39</sup> Wht3GFP<sup>8</sup> and RFamideGFP<sup>40</sup> reporters were previously generated in our lab. We used the GENEius online tool from Eurofins Genomics to codon optimize all the synthetic gene sequences for Hydractinia symbiolongicarpus. All synthetic genes were synthetized using IDT gBlocks gene

Fast fluorescent timer protein reporter (Fast-FT): The codon optimized Fast-FT coding sequence was designed in frame with P2A peptide and membrane GFP sequences (Fast-FT-P2A-GFP<sup>CAAX</sup>). The synthetic sequence was amplified by PCR and inserted into the Piwi1 (or β-tubulin) reporter plasmid<sup>5</sup> using NotI and SacI restriction enzymes. G0 colonies were bred to G2 (non-mosaic transgenic offspring). The timer property of the Fast-FT fluorescent protein (earlier blue and later red fluorescent forms according to maturation state) was aimed to differentiate i-cells (recently translated protein) from their progeny. The mature red form was detected using an mCherry filter set. However, our microscopes lacked the proper filter setup to detect the Fast-FT blue form. Thus, to identify i-cells, we calibrated the laser power to higher GFP intensities that were devoid of or low in mCherry fluorescence (Fast-FT mature red form).

Cdki1 reporter: 5' upstream and 3' downstream regulatory sequences of the Cdki1 gene (HyS0010.253) were cloned from extracted genomic DNA by PCR and inserted into an open cloning vector. Membrane GFP sequence (GFP<sup>CAAX</sup>) was placed in frame with the 5' upstream regulatory sequence. G0 colonies were bred to G2 (non-mosaic transgenic offspring).

OptoSOS: The OptoSos coding sequence<sup>25</sup> was codon optimized and designed replacing the RFP sequence by our codon optimized mScarlet fluorescent protein.<sup>8</sup> The synthetic sequence was amplified by PCR and inserted into the β-tubulin reporter construct<sup>8</sup> using Notl and Sacl restriction enzymes. We used BLAST to identify the endogenous H. symbiolongicarpus SOS catalytic domain that was amplified by PCR and inserted in frame with the SSPB sequence. Single injected embryos were grown to adult mosaic colonies, and we selected the animals who expressed the transgene in the hypostome. This procedure was repeated in Cdki1 KO animals to generate the Cdki1 KO OptoSOS line from Figure 5.

#### **CRISPR-Cas9** knockout

Single guide RNAs (sgRNAs) were designed using Geneious (2017.9.1.8) and CRISPRscan<sup>41</sup> tools. The three selected sgRNAs targeting Cdki1 did not match other genomic sequences. Modified synthetic sgRNAs were synthesized by Synthego Inc and diluted according to the manufacturer recommendations. To form the RNP complex with Cas9, the three sgRNAs were incubated together (500 ng/μL total) with recombinant Cas9 (1 μg/μl; IDT, Cat. #1074181) for 15 min at RT prior to being microinjected into zygotes.

#### Single polyp genomic DNA extraction

Protocol was adapted from ref. 8. A single polyp was isolated from a colony and transferred to 1.5 mL Eppendorf tube. The polyp was suspended in 50 µL Lysis buffer (10 mM Tris pH 8.0, 10 mM EDTA, 2% SDS), flicked several times, supplemented with 50 µL of digestion buffer (10% SDS, 0.4 mg/mL Proteinase K), and incubated at 56°C for 2–3 h with occasional flicking. Then, 100 μL of cold phenolchloroform (pH 8.0) was added. Samples were centrifuged at maximum speed for 15 min at 4°C, and supernatant was transferred to a new tube. Genomic DNA precipitation was carried out overnight at -20°C by adding two volumes of isopropanol and 1:10 total volume of Sodium Acetate Solution (3 M). Samples were cleaned up at 4°C by centrifugation and a 70% Ethanol wash. Extracted genomic DNA was dried out, resuspended in 10 μL nuclease-free water, and stored for further genotyping PCR.

## **Cell Reports**Article



#### **Genotyping CRISPR-Cas9 knockouts**

One hundred CRISPR-Cas9 larvae that had been injected as zygotes were metamorphosed and grown into small colonies. Of these, forty animals were analyzed for *Cdki1* mutations. Primers spanning the entire coding region of the gene were used in a PCR reaction to identify large deletions. We kept and grew eight G0 mosaic colonies to sexual maturity and crossed one male with a wild-type female. One hundred G1 animals were metamorphosed, grown to small colonies, and genotyped. Two sets of primers were used to identify heterozygous colonies carrying the genomic deletion: one spanning the entire coding region and another internal primer targeting the deleted intron. PCR products of heterozygous colonies were cloned into PGEMT-easy vector and sequenced using the T7 and SP6 primers (Data S3). Each of these animals was a heterozygote carrying a 3' deletion mutation in one *Cdki1* allele at the predicted cut sites and one wild type allele. One male and one female were crossed and G2 offspring were genotyped identifying five mutant homozygous animals. We performed genotyping on these animals from two independent DNA extractions and confirmed the mutation by sequencing.

#### **SABER-FISH**

Oligo probes were prepared according to<sup>34</sup> using hairpins 27 and 30. Tissue was fixed and dehydrated as previously described in<sup>8,40</sup>: Tissue samples were incubated for 15 min in 4% MgCl2 (in 50% distilled water/50% filtered seawater) and fixed in two steps. Fixative one: ice-cold 0.2% glutaraldehyde (stock: 25%, Sigma-Aldrich; G5882), 4% paraformaldehyde (stock: 16%, Alfa Aesar; 43368) in filtered seawater for 90 s. Fixative two: 4% paraformaldehyde in in PBS-0.1% Tween (PTW) for 1 h at 4°C. After three quick washes with PTW, samples were dehydrated in increasing concentrations of methanol in PTW and processed immediately by incubating in 1% H<sub>2</sub>O<sub>2</sub> diluted in 100% MeOH (ice-cold) for 45 min at 4°C. Followed by 2 quick washes with ice-cold 100% MeOH, samples were permeabilized in 75% acetone in 25% methanol and rehydrated into PTW. Two washes with glycine in PTW (2 mg/mL, 5min each; Fisher Scientific; BP381-1) followed by three PTW washes at RT. Samples were then washed three times with 1% (vol/vol) Triethanolamine pH 8.0 (TEA) in PTW for 5 min 6  $\mu$ L and 12  $\mu$ L of acetic anhydride were added to the second and third TEA washes, respectively. Samples were then rinsed with PTW and incubated in pre-warmed Whyb buffer (2×SSC pH 7.0, 1% Tween 20, 40% Formamide) at 43C for 10 min. Pre-hybridization and following steps were performed using pre-warmed reagents at 43C according to.<sup>34</sup> Whyb buffer was replaced with Hyb1 buffer (2×SSC pH 7.0, 1% Tween 20, 40% Formamide, 10% Dextran sulfate) and incubated at 43C overnight (pre-hybridization). Samples were transfer to Hybe buffer (40% Formamide, 5x SSC, 0.05 mg/mL Heparin, 0.25% Tween 20, 1% SDS, 1 mg/mL Salmon Sperm DNA, 1 mg/mL Roche blocking buffer powder) containing oligo probes at a concentration of 1 µg/120µL and hybridized for two days at 43C. Probes were removed and replaced with Whyb buffer for 10 min, followed by two washes with Whyb buffer (30 min each), a 10 min wash with 50% Whyb buffer in 2x SSCTw (2×SSC pH 7.0, 0.1% Tween 20), and two washes with 2X SSCTw (10 min each). Then, 2x SSCTw was replaced with PTW (two quick washes). Samples were warmed up to 37C, prewarmed Hyb2/fluor solution (1×PBS, 0.2% Tween 20, 10% Dextran sulfate/10 μM Fluor Oligo) was added and incubated for 1 h at 37C. Hyb2/fluor solution was replaced with pre-warmed Whyb2 (1×PBS, 0.1% Tween 20, 30% Formamide) for a 10 min incubation at 37C followed by two washes of 5 min each with PTW. Nuclear staining was then performed at RT by diluting Hoechst in PTW (1:2000) and incubating the samples for 45-60 min at RT. Samples were then quickly washed twice with PTW and mounted in 97% TDE. Samples were imaged within 4 days.

#### **Optogenetics**

Isolated hypostomes from OptoSOS transgenic animals were exposed to 12 h of constant blue illumination using a ReefLed<sup>TM</sup> 50 (RedSea) lamp. Exposure time, light intensities, and distance from the light source (6 cm) was determined experimentally to optimal survival rate. Higher intensity values and longer exposure times resulted in lethality. Two control experiments were carried out along-side the light induction: (1) OptoSOS isolated hypostomes under dark conditions, and (2) wild type hypostomes exposed to blue light. After the light induction period, samples were incubated without blue light until day 6 post amputation and fixed for immunofluorescence.

#### **Drug treatments**

We incubated isolated hypostomes in 1  $\mu$ M of Rapamycin (Sigma-Aldrich; 553210) or 1  $\mu$ M of Navitoclax ABT-263 (MedChemExpress; HY-10087) for 28 h. We determined this concentration empirically. Controls were incubated in equivalent concentrations of DMSO. Treatment time was determined experimentally to optimize survival rates. A portion of the samples was fix at 24 h post amputation for SpiDER-Gal staining. After treatment, samples were rinsed with fresh seawater, incubated until day 6 post amputation, and fixed for Immunofluorescence.

#### **Cellular staining**

Immunofluorescence (IF) staining was performed as previously described in <sup>8</sup>: the tissue was fixed in 4% Formaldehyde, 10 µL/mL Acetic acid (glacial) in filtered seawater (FSW) for 90 min at RT, followed by three washes with 1X PBST (20 min each). PBST was replaced with 5% normal goat serum (NGS; diluted in PBST) and fixed samples were blocked for 1 to 2 h at room temperature with gentle rocking. Primary antibodies were diluted in 5% NGS to desired concentration (anti-Piwi1 1:500; anti-mCherry 1:100). Blocking solution was removed, replaced with primary antibodies diluted in NGS, and incubated overnight at 4C. Samples were washed three times with PBST (10 min each), secondary antibodies were then applied (1:250 in 5% NGS) and incubated for 2 h





at RT. Tissue was rinsed with PBST and stained with Hoechst (20 mg/mL) 1:2000 in 1X PBST for 15 min, washed with 1X PBST, and mounted for imaging.

#### **EdU** staining

EdU staining was done as previously described in. 5 Isolated polyps and hypostomes were incubated in 0.01 mM EdU in FSW for 30 min, rinsed with FSW and incubated in MgCl<sub>2</sub> before fixation. Hypostomes were incubated in EdU for 2 days (3-4 dpa). Samples were fixed in 4% Formaldehyde, 10 µL/mL Acetic acid (glacial) in FSW for 90 min at room temperature (RT) and washed once with 3% BSA in PBST for 30min. Next, two washes with PBST for 1 h and 30 min, respectively, followed by two washes with 3% BSA in PBST (5 min each). The tissue was then incubated in Click-iT cocktail for 30 min, followed by three washes of 3% BSA in PBST (20 min each).

#### **TUNEL** labeling

TUNEL assays were performed using TM red In Situ Cell Death Detection Kit (#12156792910, Roche). Samples were fixed in 4% PFA in FSW for 90 min, then washed three times with PBS 0.01%Triton for 15 min, permeabilised with PBS 0.5%Triton for 90 min, and washed three times with 3% BSA in PBS for 15 min. Samples were incubated for 45 min at 37°C in a 50μL mix composed of 25 μL of reaction mix (Enzyme solution plus Label solution) and 25 µL of 3% BSA in PBS. Negative controls were incubated in Label solution only and positive controls were incubated for 25 min at 37°C in DNAse I solution (Thermo Fisher Scientific, #EN0521) prior to incubation in reaction mix only. After the reaction, samples were washed in PBS and nuclei stained using Hoechst.

#### **Imaging**

Confocal images for IF and SABER-FISH were collected using an inverted Olympus Fluoview 1000 and Olympus Fluoview 3000 laser scanning confocal microscopes.

For in vivo imaging, polyps from transgenic colonies were embedded in 0.8% low-melt agarose in filtered ASW and incubated in 35 mm imaging dishes with a glass bottom (Ibidi; D 263). Andor spinning disc and Olympus Fluoview 1000 laser scanning confocal microscopes were used to generate time-lapse movies and specific time point images. Raw images were visualized and analyzed using ImageJ/Fiji software and imaris viewer. Final figures were assembled using Adobe Illustrator and Adobe Photoshop.

Images were imported into Adobe Photoshop and their brightness and contrast adjusted as a whole. They were then imported into Adobe Illustrator to generate composite figures. We aimed at presenting all animals with their oral pole up. For this, some images (in Figures 1, 2, and S1) were rotated in their panels in Illustrator. The remaining white corners were adjusted to the background of the original image for esthetic reason. Figure S6A was composed of multiple, unmanipulated and partially overlapping images.

Piwi1 is expressed exclusively in i-cells. However, residual mRNA, protein, and the corresponding GFP reporter are present in decreasing concentrations in their progeny. Hence, we calibrated the laser power to higher Piwi1+ intensity signals using an intact polyp. We repeated this procedure prior to every acquisition to discriminate between i-cells (higher intensities) and their progeny (lower intensities).

#### Phylogenetic analysis

Multiple amino acid alignments were generated with MAFFT 7 using default parameters. Gaps were removed using Gblocks 0.91b. Final alignments were composed of 1022, 155, and 174 amino acids for mTOR alignment, P53 family alignment, and CDKI family alignment, respectively. We used PhyML with maximum-likelihood method and 1000 bootstrap replicates. The best amino acid evolution models to conduct analysis were determined, using MEGA11, to be the LG model for mTOR and P53 family alignment, and the JTT model for CDKI family alignment. Bayesian analyses were performed using MrBayes (v3.2.6) under mixed model. One-fourth of the topologies were discarded (burn-in values), and the remaining ones were used to calculate the posterior probabilities. Bayesian analysis for mTOR, P53 family, and CDKI family ran for 200,000 generations with 5 randomly started simultaneous Markov chains (MC), 500,000 generations with 10 MC, and 3,000,000 with 15 MC, respectively. For all analyses, the first chain was a cold chain and the others were heated chains.

#### **QUANTIFICATION AND STATISTICAL ANALYSIS**

Stained cells of fixed hypostomes were counted with the Fiji cell counter tool using the raw source data. Statistical analyses were executed using GraphPad prism software. We plotted the cell numbers of the different conditions and differences were assessed by comparing medians using Mann-Whitney U test.